

Parameter Estimation for the Jiles-Atherton Model in Weak Fields

Vijn, Aad R.P.J.; Baas, Olivier; Lepelaars, Eugene

DOI

[10.1109/TMAG.2020.2971435](https://doi.org/10.1109/TMAG.2020.2971435)

Publication date

2020

Document Version

Final published version

Published in

IEEE Transactions on Magnetics

Citation (APA)

Vijn, A. R. P. J., Baas, O., & Lepelaars, E. (2020). Parameter Estimation for the Jiles-Atherton Model in Weak Fields. *IEEE Transactions on Magnetics*, 56(4), Article 8979404. <https://doi.org/10.1109/TMAG.2020.2971435>

Important note

To cite this publication, please use the final published version (if applicable). Please check the document version above.

Copyright

Other than for strictly personal use, it is not permitted to download, forward or distribute the text or part of it, without the consent of the author(s) and/or copyright holder(s), unless the work is under an open content license such as Creative Commons.

Takedown policy

Please contact us and provide details if you believe this document breaches copyrights. We will remove access to the work immediately and investigate your claim.

Parameter Estimation for the Jiles–Atherton Model in Weak Fields

Aad R. P. J. Vijn¹, Olivier Baas², and Eugene Lepelaars³

¹Delft Institute of Applied Mathematics, Delft University of Technology, 2600 Delft, The Netherlands

²Maritime and Transport Technology, Delft University of Technology, 2600 Delft, The Netherlands

³Netherlands Organisation for Applied Scientific Research, 2509 The Hague, The Netherlands

The purpose of this article is to estimate the parameters of the Jiles–Atherton hysteresis model, based on minor-loop measurement data in weak applied fields. The well-known hysteresis model by Jiles and Atherton serves as a basis of this article with an extension for the closure of minor loops. In order to represent minor loops correctly, a dissipative factor is introduced. A methodology to obtain the initial magnetization of a specimen is defined, based on an expansion in terms of higher order Gaussian functions. The methodology is implemented within a finite-element method using an interconnection between MATLAB and COMSOL. This interconnection allows the investigation of potentially large ferromagnetic objects to be calibrated to the proposed ferromagnetic model in weak fields. The proposed methodology was verified using an original approach. The approach relies on the use of a sensor array that makes it possible to detect local variations of magnetic properties in steel plates. Material parameters for our test specimen are successfully obtained by means of experimental data, using the shuffled frog leaping optimization algorithm. An analysis of the obtained results shows that the calibrated model is able to represent the measurement data accurately.

Index Terms—Dissipative factor, experimental validation, ferromagnetism, hysteresis, initial magnetization, inversion, Jiles–Atherton model, minor-loop closure, parameter estimation, steel sheets.

I. INTRODUCTION

ACCURATE modeling of ferromagnetic behavior requires a complete representation of the material hysteresis properties. Over the past century, a large number of phenomenological and mathematical–physical models were presented to describe this behavior, with various successes. Well-known examples are the mathematical models by Della Torre [37], Play & Stop models [3], [28], [29], the hysteresis model proposed by Tellinen [35] and Ziske and Bödrich [44], a simple formalism that is based on physics-based concepts described by Jiles and Atherton [17] and Zirka *et al.* [43], the energy-variational model by Henrotte and Hameyer [12], François-Lavet [24], and Prigozhin *et al.* [30] and simplistic models such as the hysteresis model by Kachniarz *et al.* [20]. It is interesting to note that the Rayleigh model is related to the Preisach model [14], while the Play & Stop models are a generalization of the Preisach methodology.

These models each have their own challenges and advantages considering the representation of the model of the nature of ferromagnetism, numerical stability of implementations and effective descriptions of parameter estimation algorithms. All are able to capture a large portion of the nonlinear ferromagnetic behavior, while for a subset of these models extensions to temperature, and temporal- and stress-related effects are known. However, if one analyzes the numerical stability of the proposed models, it can be observed that, for example, implementations of the Rayleigh and Jiles–Atherton model exhibit numerical difficulties, as the magnetic field \mathbf{H}

can change of value rapidly as a response of material to its magnetizing field. Sophisticated numerical solvers are then necessary to obtain stable integration of these models by, for example, incorporating an inner-iterative scheme that stabilizes the numerical integration. Such an inner-iterative scheme is also proposed for the energy-variational model [30].

One drawback of the Jiles and Atherton model is that the model results lead to properties that are not observed in the experimental data. In the original model, minor loops are not closed which leads to unfavorable behavior in the hysteresis curve as the model encounters difficulties in representing a hysteresis curve. In [1], [4], [7], [8], [15], [17], [22], and [27], the authors address and discuss possible modifications to the Jiles and Atherton model to resolve this issue. In contrast, Preisach modeling, the Play & Stop models and the Energy-variational model (and others) ensure minor loop closure.

In more detail, the following adjustments have been proposed to the model of Jiles and Atherton to resolve the above-mentioned issue. Jiles and Atherton [17] proposed a modification of the differential equation that describes the irreversible component of the magnetization, Carpenter [4] describes scaling factors to ensure closure of minor loops. Furthermore, in the original paper of Jiles and Atherton [17] the dependencies of the material parameter k on the magnetization are discussed. It seems that taking k constant leads to such nonclosure behavior too. Leite *et al.* [27] introduced a slight modification of the irreversible component of the magnetization in order to close minor loops. By introducing a dissipative factor R in the differential equation that describes irreversible magnetization, it is possible to properly close minor loops. In particular, the factor R depends on the magnetic field value at a reversal point of a minor loop. We will refer to this modified version of the model by Jiles and Atherton as the **JA+R** model, to emphasize the addition of this dissipative

Manuscript received September 6, 2019; revised November 6, 2019 and December 22, 2019; accepted January 17, 2020. Date of publication February 3, 2020; date of current version March 18, 2020. Corresponding author: A. R. P. J. Vijn (e-mail: a.r.p.j.vijn@tudelft.nl).

Color versions of one or more of the figures in this article are available online at <http://ieeexplore.ieee.org>.

Digital Object Identifier 10.1109/TMAG.2020.2971435

0018-9464 © 2020 IEEE. Personal use is permitted, but republication/redistribution requires IEEE permission.

See <https://www.ieee.org/publications/rights/index.html> for more information.

factor R . This extended hysteresis model will serve as our choice of the model throughout this article.

In order to find a good fit between measured hysteresis curves and a hysteresis model, a parameter fit algorithm is required to find the optimal material parameters. Many numerical procedures and algorithms have been explored and proposed [18], [27], [33], [42]. This is a challenging problem because of the nonlinear nature of hysteresis. It is common practice to consider the major hysteresis loop for the determination of the parameters. However, obtaining the major loop of a specimen requires the application of large applied field strengths which imposes extra requirements on the measuring equipment. It is also likely that such procedures severely limit the size of a specimen that can be investigated. There are numerous papers concerning parameter estimation, for example, parameter estimation for JA [1], [10], [11], [27], [39] and estimation of the parameters of Play & Stop models [28], [29] in which the authors use slightly minor hysteresis loop measurement data because of the difficulty in measuring major hysteresis curves due to either the strong demagnetizing fields or the required applied field strengths. Among these papers, optimization algorithms are proposed to find a feasible set of parameters in the JA model. It has been observed that the genetic algorithm showed effective applications in finding these sets of parameters. However, one should be careful with applying the genetic algorithm, as the convergence may only be local.

The main contribution of this article is the following. Using $\mathbf{JA} + \mathbf{R}$, we have developed a methodology that estimates the material parameters in the $\mathbf{JA} + \mathbf{R}$ model based on minor loop hysteresis curve measurements. This methodology is applied on large ferromagnetic objects, such as square steel plates; other geometrical shapes and ferromagnetic materials are also possible. Furthermore, we assume that the material parameters are uniform over the domain of the object and we assume the material is anisotropic (though the proposed methodology is defined for the general case of inhomogeneous and anisotropic material). Therefore, only a small number of material parameters are sought. Based on the measurements of minor loops, in which we vary the weak background field in the order of a few hundred microtesla, an estimation of the material parameters and the dissipative factor is done using a population-based search algorithm, which searches for a global optimum.

It is important to note that the current choice of the hysteresis model is not a core aspect of this methodology. In principle, it is possible to use alternative hysteresis models for which the parameters can be estimated using the same scheme. The emphasis in the current paper is on the determination of material parameters in weak fields. All aspects of this proposed methodology are implemented in the finite-element software package Comsol Multiphysics and controlled by MATLAB.

This article has the following structure. In Section II-A, the methodology used in the proposed formalism is discussed.

In Section II-B, we give the general PDE that describes the temporal evolution of the magnetization. In Section II-C, we propose a method to determine the magnetization

distribution based on measurements and a collection of higher order Gaussian functions. This class of radial basis functions can be used to describe magnetization globally. In Section II-D, we define a parameter estimation method to determine the material properties of a ferromagnetic body. This parameter estimation method is based on measurement data of minor loops and the shuffled frog leaping algorithm (SFLA) [31].

In Section IV, we apply the proposed methodology to a collection of ferromagnetic specimens to obtain a set of material parameters for $\mathbf{JA} + \mathbf{R}$. This is based on both the determination of the initial magnetization distribution and the optimization solver SFLA. We analyze the results and the behavior of the optimization process.

In Section V, we conclude this article and discuss future recommendations. The appendixes contain an extra explanation about the proposed algorithm based on a flowchart diagram and a table in which values can be found that are used to bound the search space for the chosen numerical solver.

ASSUMPTIONS

Throughout this article, the following assumptions hold.

- 1) *Uniform background field* in the vicinity of the geometry.
- 2) *Anisotropic material*, where tensors are given by diagonal matrices hence only the principal axes are taken into account.
- 3) *Homogeneous material*, i.e., the material parameters do not depend on the location inside the geometry. This assumption reduces the complexity of the problem at stake significantly.

II. FERROMAGNETIC HYSTERESIS

In this section, a brief recap on the hysteresis model of Jiles and Atherton is given. For more details, see [2], [17], [27], [32], and [37]. The main result of this section is an adapted Jiles and Atherton model, which we call the $\mathbf{JA} + \mathbf{R}$ model, that includes both the magneto-mechanical effect up to elastic deformations and the possibility to close minor loops. Closing minor loops is essential for an accurate estimation of material parameters described in Section II-D, based on minor loop measurements.

The starting point is the definition of the effective field. The effective field reads

$$\mathbf{H}_e = \mathbf{H} + \mathbf{H}_m \quad (1)$$

where \mathbf{H} is the total magnetic field in [A m^{-1}], $\mathbf{H}_m = \alpha \mathbf{M}$ is the Weiss field in [A m^{-1}], and α is the field parameter. The magnetization \mathbf{M} is due to magnetic domain motion and is given in [A m^{-1}]. Note that the total field is considered inside the material. Therefore, the magnetic field \mathbf{H} reads

$$\mathbf{H} = \mathbf{H}_a + \mathbf{H}_d \quad (2)$$

where \mathbf{H}_a is the applied background field and \mathbf{H}_d is the demagnetizing field. Note that the value of the demagnetizing field depends on the position within the ferromagnetic body and follows from finite-element computations [16], [19].

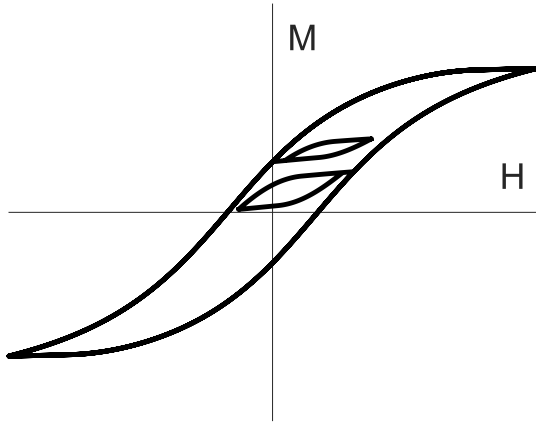


Fig. 1. Illustration of non-closure of minor loops in the model of Jiles and Atherton. Here, two minor loops are shown on both the increasing and decreasing branch of the minor loop. Non-closure of the minor loop is observed as the endpoint of the minor loop does not coincide with the starting point of the minor loop.

1) *Anhysteretic and (ir)Reversible Magnetization*: When a material starts in the demagnetized state, the ferromagnetic behavior is described by the anhysteretic magnetization curve. The anhysteretic magnetization curve in the i th direction reads

$$(\mathbf{M}_{\text{an}}(\mathbf{H}_e))_i = (M_s)_i \mathcal{L}\left(\frac{\|\mathbf{H}_e\|}{a_i}\right) \frac{(H_e)_i}{\|\mathbf{H}_e\|}, \quad i \in \{x, y, z\} \quad (3)$$

where $\mathcal{L}(x) = \coth(x) - 1/x$ is the Langevin function, $(M_s)_i$ is the saturation magnetization value in $[\text{A m}^{-1}]$ in the i th direction and a_i is a constant in $[\text{A m}^{-1}]$.

The magnetization is considered the sum of a reversible component \mathbf{M}_{rev} and irreversible component \mathbf{M}_{irr}

$$\mathbf{M} := \mathbf{M}_{\text{irr}} + \mathbf{M}_{\text{rev}}, \quad \mathbf{M}_{\text{rev}} = \mathbf{c}(\mathbf{M}_{\text{an}} - \mathbf{M}_{\text{irr}}) \quad (4)$$

where \mathbf{M}_{irr} and \mathbf{M}_{rev} are in $[\text{A m}^{-1}]$, and \mathbf{c} is the domain rotation loss matrix. Note that when $\mathbf{c} = \mathbf{I}$, then \mathbf{M} is completely reversible and $\mathbf{M}_{\text{irr}} = \mathbf{0} = \mathbf{0}$.

2) *Dissipative Factor for Minor-Loop Closure*: The non-closure of minor loops in the model by Jiles and Atherton is an artifact that shows a lack of resemblance of \mathbf{JA} compared to experimental data. As an example, a hysteresis curve and two minor loops are shown in Fig. 1, based on \mathbf{JA} .

In [27], a dissipative factor is introduced that is used to close minor loops in the traditional Jiles and Atherton formalism. Note that the value of the dissipative factor for a minor loop depends on the amplitude of the corresponding applied field. The adapted differential equation [2] describing vectorial behavior of the irreversible magnetization reads

$$d\mathbf{M}_{\text{irr}} = [\boldsymbol{\chi}^{-1}(\mathbf{M}_{\text{an}} - \mathbf{R}\mathbf{M})d\mathbf{H}_e]^+ \quad (5)$$

where $\boldsymbol{\chi}$ and \mathbf{R} are diagonal matrices given by

$$\boldsymbol{\chi} = \begin{bmatrix} \chi_1 & 0 & 0 \\ 0 & \chi_2 & 0 \\ 0 & 0 & \chi_3 \end{bmatrix} \quad \text{and} \quad \mathbf{R} = \begin{bmatrix} R_1 & 0 & 0 \\ 0 & R_2 & 0 \\ 0 & 0 & R_3 \end{bmatrix}. \quad (6)$$

Here, $R_i > 0$ are dissipative factors and $\chi_i = k_i \delta_i$ where k_i is the pinning parameter in $[\text{A m}^{-1}]$ in the i th direction and δ_i is the sign of the slope of the i th component of the effective field, $\delta_i = \text{sign}(d(\mathbf{H}_e)_i)$. Furthermore, $[x]^+ := \max\{0, x\}$ is recognized as the linear activation function.

3) *Anisotropic Material*: In this article, the simplest case of anisotropic material is considered, i.e., only along the principal axes inside the material, behavior may differ. This implies that the domain rotation loss \mathbf{c} and the field parameter $\boldsymbol{\alpha}$ takes on the following form:

$$\mathbf{c} = \begin{bmatrix} c_1 & 0 & 0 \\ 0 & c_2 & 0 \\ 0 & 0 & c_3 \end{bmatrix} \quad \text{and} \quad \boldsymbol{\alpha} = \begin{bmatrix} \alpha_1 & 0 & 0 \\ 0 & \alpha_2 & 0 \\ 0 & 0 & \alpha_3 \end{bmatrix}. \quad (7)$$

Note that the anisotropy assumption is already reflected in the definitions of $\boldsymbol{\chi}$ and \mathbf{R} .

A. General Form of PDE for $\mathbf{JA} + \mathbf{R}$

Based on the modeling principles discussed in the previous sections, the $\mathbf{JA} + \mathbf{R}$ hysteresis model is defined. The general partial differential equation describing the temporal evolution of $\mathbf{M}(t)$ in time reads

$$\frac{d\mathbf{M}}{dt} = \mathbf{c} \frac{d\mathbf{M}_{\text{an}}}{dt} + (\mathbf{I} - \mathbf{c}) \frac{d\mathbf{M}_{\text{irr}}}{dt} \quad (8)$$

for a given *initial magnetization distribution* $\mathbf{M}|_{t=0} = \mathbf{M}_0$. For numerical consistency, it is necessary to indicate the value of $\delta_i(t=0)$ because the slope of the effective field is unknown at $t=0$. We choose this value based on the right derivative of the applied field \mathbf{H}_a , that is

$$\delta_i(t=0) \equiv \lim_{t \downarrow 0} \frac{(\mathbf{H}_a)_i(t) - (\mathbf{H}_a)_i(0)}{t} \quad (9)$$

where we tacitly assume that this signal is known *a priori*.

The derivative of $\mathbf{M}_{\text{irr}}(t)$ with respect to t follows from (5) after differentiation with respect to t :

$$\frac{d\mathbf{M}_{\text{irr}}}{dt} = \left[\boldsymbol{\chi}^{-1}(\mathbf{M}_{\text{an}} - \mathbf{R}\mathbf{M}) \frac{d\mathbf{H}_e}{dt} \right]^+ \quad (10)$$

Note that (10) follows easily after applying the chain rule:

$$\frac{d\mathbf{M}_{\text{irr}}}{dt} = \left(\frac{\partial \mathbf{M}_{\text{irr}}}{\partial \mathbf{H}_e} \right) \frac{d\mathbf{H}_e}{dt} \quad (11)$$

to (5) for both cases $[x]^+ = 0$ and $[x]^+ = x$ to yield (10).

III. INITIAL MAGNETIZATION DISTRIBUTION \mathbf{M}_0

1) *General Approach*: The initial magnetization distribution is, in general, unknown. In order to find or approximate the magnetization initially, an inverse problem has to be solved. Solving inverse problems in magnetostatics is a challenging task [5], [6], [40], [41], which often requires additional regularization techniques for stable solutions. However, in the proposed approach below no regularization is considered.

Defining an inverse problem for finding the magnetization distribution is typically based on a finite-element method approach. In such cases, the magnetization is described by local basis functions. Typical choices for such basis functions are zeroth order (constant functions) and linear basis functions. Higher order basis functions are usually avoided because of their complexity. Another argument is that higher order basis functions tend to be too smooth and, therefore, fall short in representing the solution space for \mathbf{M} .

Here, we propose a “global approach” for finding \mathbf{M} . The magnetization distribution is described by a collection of

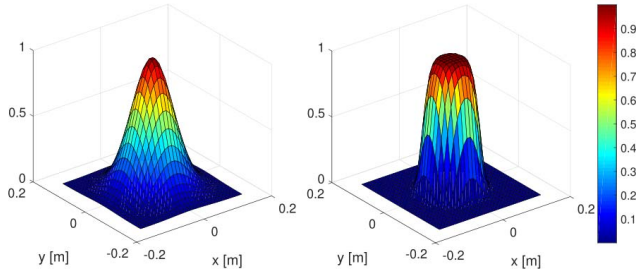


Fig. 2. Two examples of higher order Gaussian functions, $A = 1$ and $P_x = P_y = 1$ (left) and $A = 1$ and $P_x = P_y = 3$ (right).

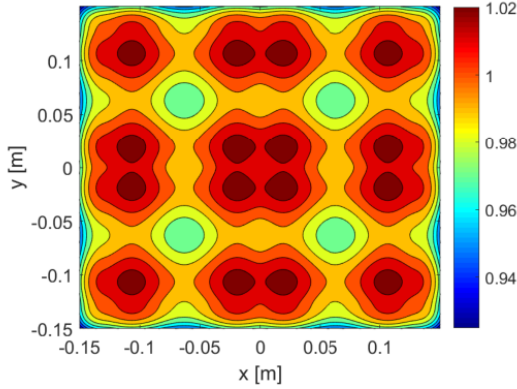


Fig. 3. Example of a distribution of nine 2-D higher order square Gaussian functions, $\sigma_x = \sigma_y = 0.05$, $P_x = P_y = 1.5$ and $A = 1$ for all Gaussian functions.

higher order Gaussian functions.¹ A higher order rectangular Gaussian function in 2-D with amplitude $A \in \mathbb{R}$, center (x_c, y_c) and spreads $\sigma_x, \sigma_y > 0$ reads

$$f(x, y) = A \exp \left(- \left(\frac{(x - x_c)^2}{2\sigma_x^2} \right)^{P_x} - \left(\frac{(y - y_c)^2}{2\sigma_y^2} \right)^{P_y} \right). \quad (12)$$

Here, the powers P_x and P_y are used to control the decay of the function. Larger values for P_x and P_y lead to a flat-top and a rapid Gaussian fall-off to zero. Two examples of these higher order Gaussian functions are given in Fig. 2. Notice that in the limit as $P_x, P_y \rightarrow \infty$, higher order Gaussian functions correspond to basis functions with compact support. An example of a collection of Gaussian functions is given in Fig. 3, which can be used to approximate any constant function defined on a (square) domain. This choice of global functions also allows us to introduce magnetic anomalies inside a magnetized object.

2) *Determination of \mathbf{M}_0* : In the remainder of this section, without loss of generality, consider a magnetized plate Ω . Furthermore, assume *a priori* that centers $(x, y) \in \Omega$, spreads $\sigma_x, \sigma_y > 0$ and the powers $P_x, P_y > 0$ are fixed for a collection of Gaussian functions $\{f_i(A_i)\}_{i=1}^n$. Hence, only the amplitudes of the Gaussian functions are unknown and can be chosen freely.

¹Finally, recall the following result from Approximation Theory: for a square interval $[0, 1]^2$ the set of all Gaussian functions is dense in the function space $\mathcal{C}([0, 1]^2, \mathbb{R})$. Therefore, any component of a magnetization can be approximated with arbitrary accuracy by a collection of n Gaussian functions, for sufficiently large $n \in \mathbb{N}$.

The aim is to find the magnetization \mathbf{M} of the plate Ω . This is done based on measurements of the magnetic induction field \mathbf{B} at sensor locations surrounding the plate.

To that end, observe that a Gaussian function $f_i(A_i)$ describes a magnetization distribution $\mathbf{M}_i = f_i(A_i)\mathbf{u}_i$ on Ω , where \mathbf{u}_i is a unit vector. For example, if for all $i \leq n$ $\mathbf{u}_i = \mathbf{u}_x$, then the x -component of the magnetization is sought.

Subsequently, this magnetization produces a magnetic induction field $\mathbf{B}_i(A_i)$ in sensor locations $\mathbf{r}_1, \mathbf{r}_2, \dots, \mathbf{r}_N \in \Omega^c$. To determine the initial magnetization, the following linear problem has to be solved:

$$\hat{\mathbf{A}} = \arg \min_{A_1, A_2, \dots, A_n \in \mathbb{R}} \left\| \sum_{i=1}^n \mathbf{B}_i(A_i) - \mathbf{B}_m \right\|_2^2 \quad (13)$$

where \mathbf{B}_m is a vector that contains the measured values of the magnetic field in the sensor locations $\mathbf{r}_1, \mathbf{r}_2, \dots, \mathbf{r}_N$ and $\hat{\mathbf{A}} = [A_1, A_2, \dots, A_n]^T$ is a vector containing the optimal values for amplitudes A_1, A_2, \dots, A_n . Note that the resulting vector $\hat{\mathbf{A}}$ depends on the collected measurement data, and the sensor locations. To find the optimal sensor locations, one should vary the locations and investigate the sensitivity of the solution and fit with respect to these variations. However, finding optimal sensor locations is, in general, a very complex problem.

To obtain acceptable sensor configurations, one can derive configurations on the basis of minimization of the norm of the Fisher information matrix (FIM) method [21], [38]. Alternatively, the determinant or the trace of the FIM is also a possibility. An alternative method is to minimize the expected Bayesian loss function that uses the inverse of the FIM as a measure for the quality of the sensor configuration [34]. However, information about the (model) noise is necessary, which can be hard to obtain.

IV. PARAMETER ESTIMATION OF $\mathbf{JA} + \mathbf{R}$

In this section, we discuss the estimation of material parameters in the $\mathbf{JA} + \mathbf{R}$ model. First note that there is a total of 18 parameters that fully define the model, summed up in the following matrices:

$$\begin{aligned} \text{Jiles-Atherton} &\equiv \begin{bmatrix} \alpha_1 & \alpha_2 & \alpha_3 \\ (M_s)_1 & (M_s)_2 & (M_s)_3 \\ a_1 & a_2 & a_3 \\ c_1 & c_2 & c_3 \\ k_1 & k_2 & k_3 \end{bmatrix} \\ \text{Dissipative factor} &\equiv \begin{bmatrix} R_1 & R_2 & R_3 \end{bmatrix} \end{aligned} \quad (14)$$

where the parameters in the first, second, and third columns in (14) correspond to the ferromagnetic behavior in the x -, y - and z -directions, respectively. In the later part of this report, we assume for simplicity that the dissipative factors are constant such that the parameters can be stored in a single parameter vector, denoted by $\mathbf{p} \in \mathbb{R}^{18}$. Indeed, the values of R_1, R_2, R_3 may vary in the model.

A. Forward Problem

In this section, we define the forward problem that serves as a foundation for the derivation of the parameter estimation problem. In particular, the main result in this section is the definition of $\mathbf{B}_c[\mathbf{p}]$, which is a vector that consists of computed

magnetic induction field values at sensor locations for a given applied magnetic field signal.

Let $\mathbf{B}_d: [0, t_{\text{end}}] \rightarrow \mathbb{R}^3$ be an applied background field signal and let Ω denote a ferromagnetic object. Furthermore, assume that the initial magnetization $\mathbf{M}|_{t=0} = \mathbf{M}_0$ is known. Given a fixed set of material parameters for $\mathbf{J}\mathbf{A} + \mathbf{R}$, the solution to the forward problem is the magnetic induction field caused by the magnetization of Ω at a collection of measurement locations for $t \in [0, t_{\text{end}}]$, when the background field signal is applied to Ω .

If $\mathcal{M} = \{\mathbf{r}_1, \mathbf{r}_2, \dots, \mathbf{r}_K\}$ denotes a set of K measurement locations, then $\mathbf{B}_c(t) \in \mathbb{R}^{3K}$ is a vector that contains the magnetic induction field at the measurement locations at time $t \in [0, t_{\text{end}}]$.

If $\{t_1, t_2, \dots, t_T\} \subset [0, t_{\text{end}}]$ denotes a sample of time instants, then we may form vector $\mathbf{B}_c[\mathbf{p}] \in \mathbb{R}^{3KT}$ by concatenating the vectors $\mathbf{B}_c(t_1), \mathbf{B}_c(t_2), \dots, \mathbf{B}_c(t_T)$ at the corresponding time instances

$$\mathbf{B}_c[\mathbf{p}] = \mathbf{Vec}(\mathbf{B}_c(t_1), \mathbf{B}_c(t_2), \dots, \mathbf{B}_c(t_T)). \quad (15)$$

B. Minimization Problem

The idea behind parameter estimation is as follows: based on a collection of N measured minor loops, with T measurements per loop at K measurement locations, the task is to find a feasible collection of parameters $\hat{\mathbf{p}} \in \mathbb{R}^{18}$ such that there is a good fit between the measured minor loops, and the minor loops computed by the FEM implementation in COMSOL. To measure the fit, the residual

$$\mathbf{Res} := \mathbf{B}_m - \mathbf{B}_c[\mathbf{p}] \quad (16)$$

is chosen. Here, the vector $\mathbf{Res} \in \mathbb{R}^{3KNT}$ is the residual between the measured minor loops \mathbf{B}_m and the computed values of the minor loop $\mathbf{B}_c[\mathbf{p}]$ for a given parameter vector \mathbf{p} . If the residual is small, then corresponding parameter vector \mathbf{p} is a feasible solution to the parameter estimation problem.

To define the minimization problem, we introduce the root mean square error (RMSE)

$$\mathcal{J}(\mathbf{p}) = \sqrt{\frac{\mathbf{Res}^T W \mathbf{Res}}{n}}, \quad n \equiv 3KNT. \quad (17)$$

The positive-definite diagonal matrix W contains weights that can be used to control the importance of each measured point on the minor loop. For example, one should relax the fit near the tip points of the minor loop, to increase the performance of the parameter estimation. This is achieved by choosing weights w_{ii} relatively small for tip point measurements, compared to the weights for other measurements.

C. Solving the Minimization Problem

To find the optimal values that best fit the (measured) data, a memetic metaheuristic called the SFLA is applied [23]. The SFLA is a population-based cooperative search inspired by frogs that work together to find food. The algorithm contains both elements of local search and global information exchange, and it is shown to be very efficient for finding traditional Jiles and Atherton parameters [31].



Fig. 4. Measurement facility “CLAViS” that contains a coil configuration to change the ambient field in three directions.

Choosing a particular bounded search space increases the speed of convergence significantly. This is done by choosing suitable boundaries for the unknowns. The minimal and maximal values for the above-mentioned parameters in the $\mathbf{J}\mathbf{A} + \mathbf{R}$ model are given in Appendix A. These bounds are based on successively applying the SFLA to learn the behavior of the optimization process and the already known material parameters found in the literature [18], [25], [26], [36].

Finally, in Appendix B a flowchart is shown that describes the complete parameter estimation procedure based on the initial magnetization distribution and the SFLA.

V. MEASUREMENT SETUP

In this section, the experimental setup is explained briefly. A measurement facility is available consisting of a coil configuration and a magnetic sensor array. The rectangular coil configuration can change the local ambient magnetic field by imposing a uniform magnetic field in all three directions. Fig. 4 shows a picture of the coil structure. Inside the cage the background field can take values of the form:

$$\{\mathbf{B}_{\text{app}} \in \mathbb{R}^3 : |(\mathbf{B}_{\text{app}})_i| \leq 400 \mu\text{T for } i = x, y, z\}. \quad (18)$$

The sensor array consisting of 112 sensors is placed 56 mm below the object. To measure the magnetic field, HMC5983 Triple Axis Compass magnetometers are used. Depending on the set gain, the sensor noise is approximately 1 up to 3 μT . A schematic overview of this sensor array is found in Fig. 5.

VI. EXPERIMENTAL RESULT

In this section, we apply the proposed parameter fit to steel specimens. The goal is to obtain the material parameters for $\mathbf{J}\mathbf{A} + \mathbf{R}$. The assumptions of homogeneity and isotropy imply that there is no spatial dependence in the material parameters. Therefore five material parameters are sought, plus a dissipative factor for each measured minor loop.

A. Specimen Description

In this experiment, four different specimen (I–IV) are investigated. Each specimen is a square metal plate with sides

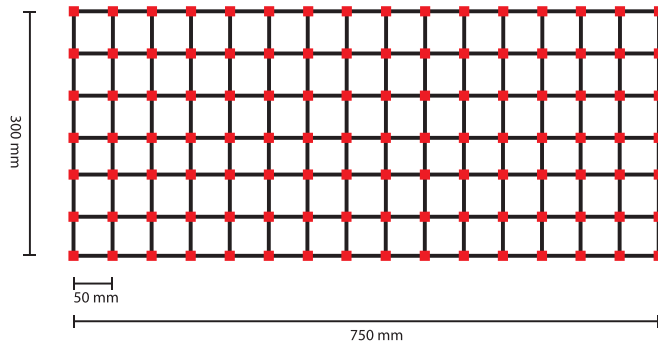


Fig. 5. Schematic overview of the sensor array.



Fig. 6. Steel plate above sensor array.

of 300 mm. Specimens I and III have a thickness of 5 mm, II and IV have a thickness of 2 mm.

Each plate is placed parallel to the sensor array in the cage and is measured at a distance of 56 mm above the array. Fig. 6 shows a steel plate within the coil structure on top of the sensor array.

In the remainder of this section, we take the measurement and results of specimen I as a guideline. The results of the other specimen are similar except for specimen III. This is likely due to the prior deperming procedure applied to this specimen, which made the initial magnetization distribution estimation procedure additionally complicated.

B. Measuring a Minor Loop

At the start of a measurement, the background field is set to $0\mu\text{T}$ in x -, y -, and z -directions, which is from here on defined as t_1 . Then, the background field is varied in the x -direction for one full period with an amplitude of μT , where $A \in \{100, 200, 300, 400\}$. During this period, five distinctive time instants are defined:

- 1) t_A , the starting point when the background field is $0\mu\text{T}$;
- 2) t_B , after the background field has been increased to μT in x -direction;
- 3) t_C , after the background field is reduced to $0\mu\text{T}$;
- 4) t_D , after the background field is set to μT in x -direction;
- 5) t_E , when the background field is increased back to $0\mu\text{T}$.

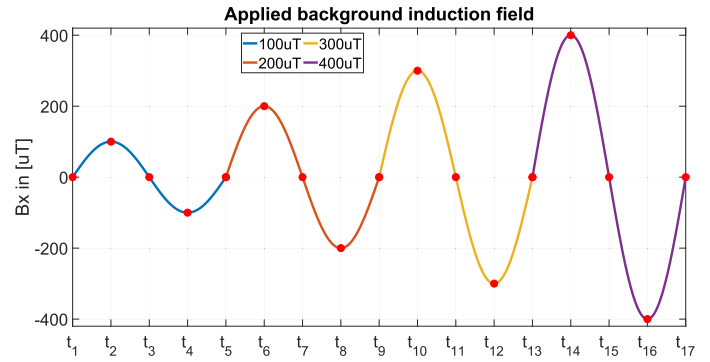
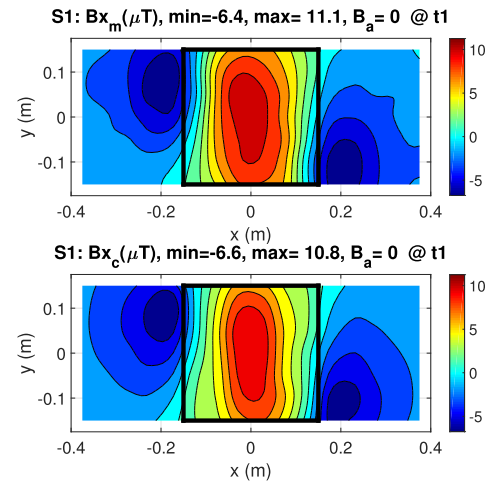


Fig. 7. Scenario: sinusoidal background field of increasing and measurements at several instances.

Fig. 8. Specimen 1. Top: measured B_x -field at t_1 . Bottom: corresponding computed B_x -field based on the initial magnetization distribution estimation.

In total, the experiment consists of measuring four minor loops subsequently. See Fig. 7 for clarification of the described scenario. The first measurement (at time $t = t_1$) is used to determine the initial magnetization distribution \mathbf{M}_0 , and we refer to Section II-C for more details on this specific routine.

C. Initial Magnetization Determination

First the initial magnetization of specimen I is determined. The measurement of the magnetic induction field (the x -component B_x) of specimen I in zero field at time $t = t_1$ is given in Fig. 8. This is a measurement in which the background field is canceled by the coil cage.

Applying the method in Section II-C leads to the following initial magnetization distribution for which the x -component of the magnetization is given in Fig. 9. Here, the collection of higher order Gaussian functions is chosen such that the resulting condition number of the linear problem is low. This is done by choosing functions that are (almost) linearly independent. By tuning the values of σ_x and σ_y such that the resulting support of the Gaussian functions is small, one can achieve such independences. Finally, solving the linear problem is done using standard Gaussian elimination (or equivalently using an LU decomposition of the coefficient matrix).

After solving the linear problem of finding the amplitudes $(A_i)_i^n$ of the Gaussian functions, the corresponding initial

TABLE I
JA + R PARAMETERS OBTAINED USING SFLA

JA Parameter	I	II	III	IV	Unit
M_s	1.52×10^6	1.67×10^6	1.52×10^6	1.66×10^6	$A\ m^{-1}$
k	379	270	295	323	$A\ m^{-1}$
a	2565	1256	1763	379	$A\ m^{-1}$
c	0.1344	0.0974	0.1139	0.1194	-
α	1.793×10^{-3}	9.929×10^{-4}	9.884×10^{-4}	7.777×10^{-4}	-
thickness	5	2	5	2	mm

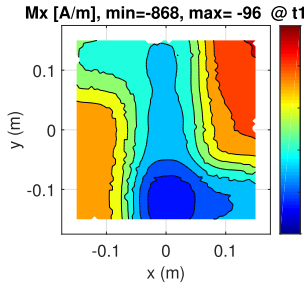


Fig. 9. Specimen 1: estimated initial magnetization at time t_1 . Only the x -component of the initial magnetization is shown, as this is the dominant component of the vector field.

magnetization distribution is found and given in Fig. 9. The erratic behavior that is seen in the initial magnetization distribution is caused by COMSOL when the solution to the linear problem was imported to COMSOL. COMSOL translates the continuous magnetization distribution to a discretized version on a mesh for further finite-element computations.

The resulting computed magnetic induction field for the obtained initial magnetization distribution is found in Fig. 8. Compared to the measured field, there is a good agreement. The difference between the computed and measured values in terms of the RMSE is sufficiently small, and therefore we accept the estimation of this initial magnetization distribution.

D. Parameter Estimation Results

Using the initial magnetization distribution from the previous subsection, the **JA + R** material properties are obtained using forward simulations within the SFLA as described in Section IV-B. The optimal parameter values for all specimen are found in Table I. In particular, the dissipative factors R for specimen I for minor loops of amplitude 100, 200, 300, and $400\ \mu\text{T}$ are, respectively, $R_{100} = 1.5$, $R_{200} = 1.2$, $R_{300} = 1.1$, and $R_{400} = 1.0$. Note that these values are consistent with the reasoning in [27], in which it is assumed that the values of R are decreasing with increasing field strength, and such that R is bounded below by 1.

It is observed that applying the SFLA multiple times on the same problem may result in different sets of parameters for which the functional takes (approximately) the same minimal value. This implies that based on minor loop measurements the set of parameters is not unique. A consequence is that these material parameters cannot be used in the region of the hysteresis curve outside the $400\text{-}\mu\text{T}$ minor loop, as it is expected that the hysteresis curve outside this region is poorly described by the obtained material parameters. Fortunately, for our applications, this is not a limitation because we stay within the $400\text{-}\mu\text{T}$ region for a given initial magnetization distribution.

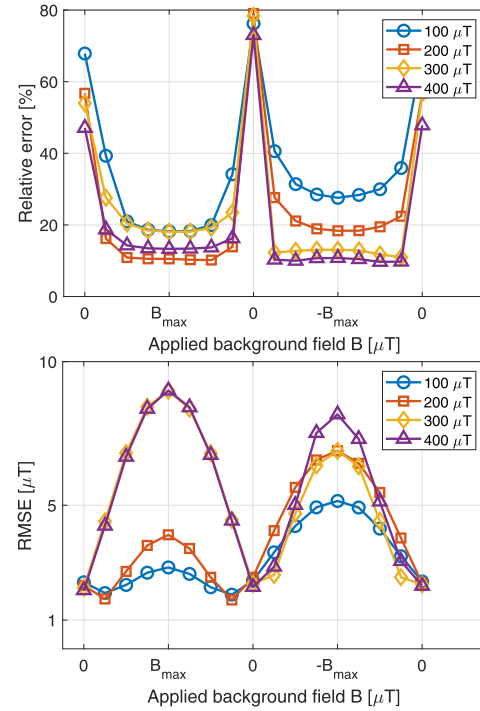


Fig. 10. Specimen 1: relative error and RMSE.

E. Error Analysis of SFLA Results

The resulting computed magnetic induction field based on the initial magnetization from Fig. 9 and optimal **JA + R** parameters from Table I subjected to a hysteresis loop of $400\ \mu\text{T}$ for specimen I is given in Fig. 11. Based on visual inspection, a good agreement is seen between the measured fields and the computed fields by the proposed model.

The result of error calculations for the first specimen is given in Fig. 10. Observe that the relative error is smaller for larger minor loops. This is explained by the fact that for larger background fields the hysteresis effects are more pronounced, such that discrepancies between the measured and computed fields are relatively small. It can be observed that, as expected, the relative error becomes rather large when the background field is zero since the measured fields are much closer to $0\ \mu\text{T}$ than whenever the background field is nonzero. Therefore, no strong conclusions can be made by interpreting the values of the relative error.

A better quantity to considering is the RMSE which averages all absolute errors along the measurement locations. Observe that this error does not exceed $2\ \mu\text{T}$ whenever the background field is zero. This error is within the sensor noise level, hence the model represents our measurements very well in these cases. Unfortunately, there is a large peak in the

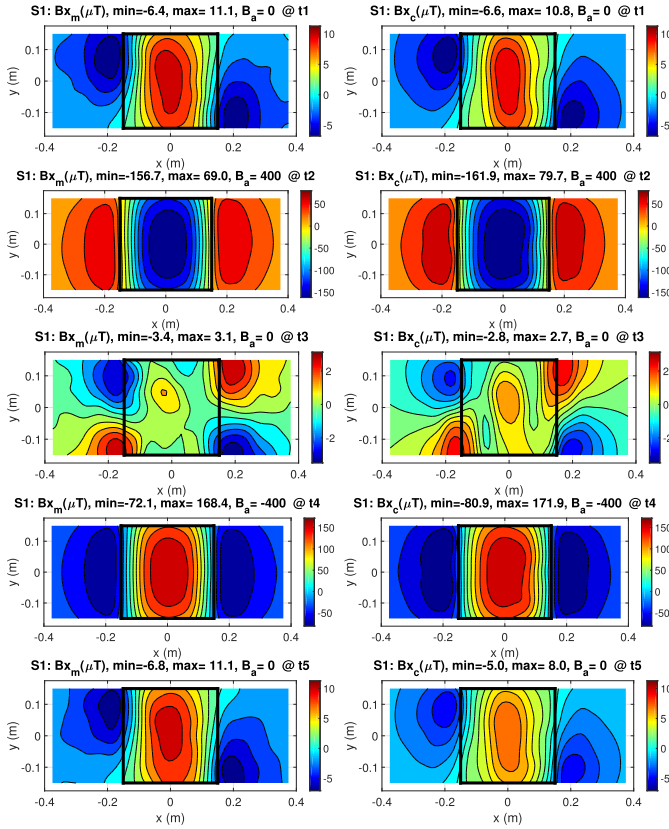


Fig. 11. Specimen 1: measured (left) and computed (right) magnetic induction field component B_x at t_A, t_B, \dots, t_E for a $400\text{-}\mu\text{T}$ minor loop measurement. Note that all field components (B_x, B_y, B_z) are used in the computations.

RMSE computed during a $400\text{-}\mu\text{T}$ minor loop. A plausible explanation for this is that an error occurred while doing a measurement and that the coil configuration did not produce the correct background field. Similar arguments may hold for other minor loops, although it is not completely clear if the larger RMSE is due to malfunctioning of the equipment or due to the performance of the model.

Note that for measurements in zero background field, there is a significant discrepancy between the measured and computed magnetic induction field. Nevertheless, there is a good agreement between the measured and computed $400\text{-}\mu\text{T}$ minor loop with a maximum RMSE error of $6\text{ }\mu\text{T}$. Overall, the RMSE is 10% (see Fig. 11) of the average measured field strength which indicates a good fit.

In general, it is also observed that there is a better agreement between the model and measurements for larger field strength amplitude. This makes sense since high amplitude field variations make larger hysteresis effects better visible. In total, based on error computations we conclude that we correctly found material parameters for the **JA + R** model and our model reproduces the measured data accurate enough.

F. Computational Effort

Finally, we look at the computational effort of SFLA. The computation time is rather long. For each specimen there are 1000 evaluations of the forward problem required within the SFLA to find a good fit. This translates to a total computation time of approximately 24 h on a high-end CPU.

TABLE II
JA + R PARAMETER BOUNDARIES FOR SFLA

JA Parameter	min. value	max. value	Unit
M_s	1.50×10^6	1.80×10^6	A m^{-1}
k	0	5000	A m^{-1}
a	0	5000	A m^{-1}
c	0.05	0.5	-
α	1.0×10^{-5}	1.0×10^{-2}	-

The computational burden is mainly caused by communication between MATLAB and COMSOL. COMSOL is used to compute the forward simulations that the SFLA requires in the optimization problem. However, each evaluation of such a forward simulation requires a fresh call to the COMSOL engine, which drastically increases the computation time. Indeed, a more sophisticated implementation of the method reduces the computation time significantly by integrating SFLA into COMSOL, so there is no need to rebuild the model every time.

VII. CONCLUSION

This article presented a method to estimate the material parameters of homogeneous anisotropic material in the Jiles and Atherton Model framework in weak applied fields. This estimation is based on both the hysteresis model that we refer to as **JA + R** and the optimization algorithm called the SFLA. Based on a collection of minor loop measurements for steel plates in weak fields, we have shown that material parameters of a number of specimen can be obtained at the required accuracy.

The choice to use only minor loop measurements is not common and we have shown that it is possible to only use such measurements with accurate results. This increases the applicability of material estimation properties, while in other related work only material parameters are obtained using major loop measurements. Such measurements are not trivial and may not be achievable in practice. Therefore, our method is applicable in finding the material parameters in a more general setting.

The material parameters that we have found are similar to values found in the literature for different alloys of steel. This gives us confidence that our application of the proposed methodology is correctly performed. Also, it is shown that the RMSE, whenever the results are compared to the measurements, is small enough. It is further noted that the performance of the method is better when the initial magnetization is not too small. Deperming a specimen increased the complexity of finding material parameters, and therefore this is an important observation for future experiments.

The first indications show that the obtained values have some predictive power to model ferromagnetic behavior for weak fields inside the region that is used to obtain the parameters. However, more research and measurements are required to further investigate this predictive power in more detail, e.g., how to interpret the nonuniqueness of obtained material parameter set, as different sets are solutions to the minimization problem as described in Section IV-B.

Future steps are to apply the methodology to experimental data to obtain the material parameters for the full anisotropic tensor case. Furthermore, the use of regularization to increase the robustness of the solutions to the parameter estimation is

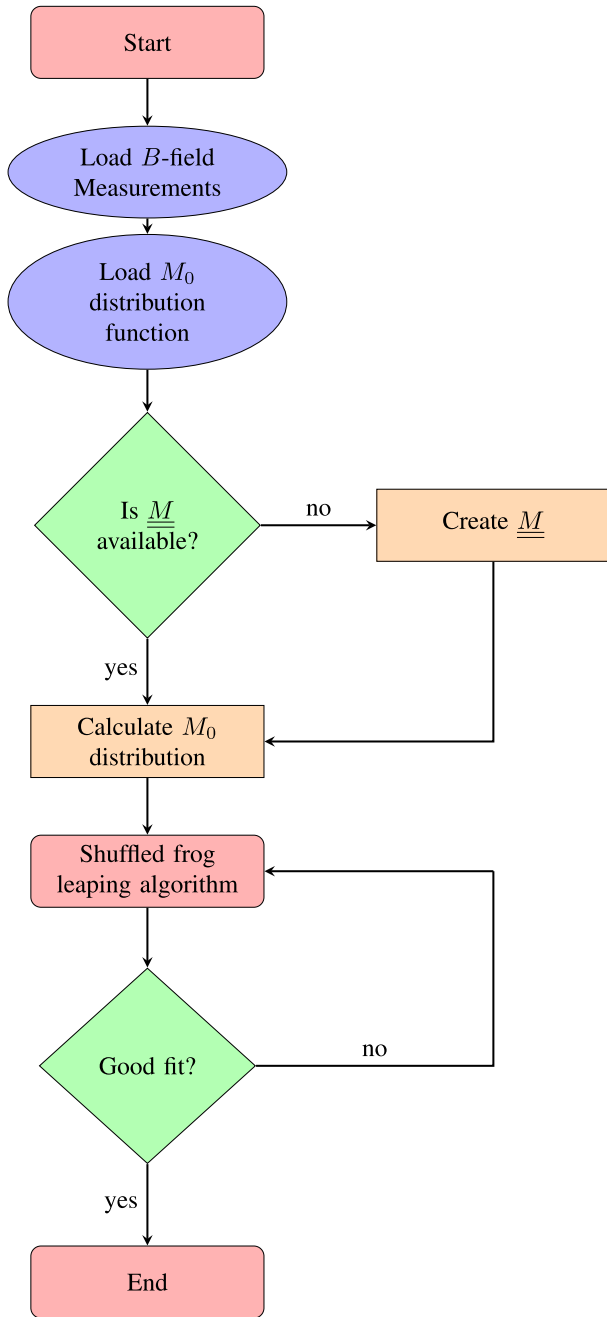


Fig. 12. Algorithm for determination of material parameters. First, measured data of the magnetic induction field B is loaded into the algorithm. Based on the initial magnetization distribution, the sensitivity matrix \underline{M} is created and M_0 is computed. Then the SFLA is used to find the optimal set of material parameters that fits the measured data in an optimal way.

valuable and must be incorporated in further extensions of the proposed model. This will reduce the effect of noise to the solutions. Lastly, the predictive performance of the obtained parameters is still ongoing research and must be understood in more detail.

APPENDIX A

TABLE OF JA+R PARAMETER BOUNDARIES FOR SFLA

A set of $\mathbf{JA} + \mathbf{R}$ parameter boundaries for SFLA are given in Table II. Recall that using such bounds reduces the computation time to execute the SFLA and speeds up the convergence of the algorithm. The values of the boundaries should be

chosen in such a way that one avoids the introduction of bias in the solution. In this article, the values are based on both known values from the literature for steel alloys, as mentioned in Section III-B.

APPENDIX B

PARAMETER ESTIMATION FLOWCHART

In this appendix, a flowchart for the proposed parameter estimation is presented. Based on the initial magnetization distribution estimation and the SFLA, an optimization process is defined to find the optimal values of the parameters in the $\mathbf{JA} + \mathbf{R}$ model. The flowchart can be found in Fig. 12.

To clarify the flowchart, note that \underline{M} is the coefficient matrix based on the collection of higher order Gaussian functions with unknown amplitudes. Note that the linear problem mentioned in (13) can be translated to a linear system of the form

$$\underline{M}\mathbf{A} = \mathbf{b} \quad (19)$$

from which the initial magnetization distribution can be computed.

ACKNOWLEDGMENT

This work was supported by the Defence Materiel Organisation, The Netherlands.

REFERENCES

- [1] A. Benabou, J. V. Leite, S. Clénet, C. Simão, and N. Sadowski, "Minor loops modelling with a modified Jiles–Atherton model and comparison with the Preisach model," *J. Magn. Magn. Mater.*, vol. 320, no. 20, pp. e1034–e1038, 2008.
- [2] A. Bergqvist, "A simple vector generalization of the Jiles–Atherton model of hysteresis," *IEEE Trans. Magn.*, vol. 32, no. 5, pp. 4213–4215, Sep. 1996.
- [3] S. Bobbio, G. Milano, C. Serpico, and C. Visone, "Models of magnetic hysteresis based on play and stop hysterons," *IEEE Trans. Magn.*, vol. 33, no. 6, pp. 4417–4426, Nov. 1997.
- [4] K. Carpenter, "A differential equation approach to minor loops in the Jiles–Atherton hysteresis model," *IEEE Trans. Magn.*, vol. 27, no. 6, pp. 4404–4406, Nov. 1991.
- [5] O. Chadebec, J.-L. Coulomb, J.-P. Bongiraud, G. Cauffet, and P. Le Thiec, "Recent improvements for solving inverse magnetostatic problem applied to thin shells," *IEEE Trans. Magn.*, vol. 38, no. 2, pp. 1005–1008, Mar. 2002.
- [6] O. Chadebec, J. Coulomb, G. Cauffet, and J. Bongiraud, "How to well pose a magnetization identification problem," *IEEE Trans. Magn.*, vol. 39, no. 3, pp. 1634–1637, May 2003.
- [7] K. Chwastek, J. Szczygłowski, and W. Wilczynski, "Modelling dynamic hysteresis loops in steel sheets," *Compel*, vol. 28, no. 3, pp. 603–612, May 2009.
- [8] K. Chwastek, "Modelling offset minor hysteresis loops with the modified Jiles–Atherton description," *J. Phys. D, Appl. Phys.*, vol. 42, no. 16, Aug. 2009, Art. no. 165002.
- [9] K. O'Grady and S. J. Greaves, "Minor hysteresis loop effects in magnetic materials," *J. Magn. Magn. Mater.*, vol. 138, pp. L233–L236, Dec. 1994.
- [10] C. Guérin, K. Jacques, R. V. Sabariego, P. Dular, C. Geuzaine, and J. Gyselinck, "Using a Jiles–Atherton vector hysteresis model for isotropic magnetic materials with the finite element method, Newton-Raphson method, and relaxation procedure," *Int. J. Numer. Model.*, vol. 30, no. 5, p. e2189, Sep. 2017.
- [11] M. Hamimid, S. Mimoune, and M. Feliachi, "Minor hysteresis loops model based on exponential parameters scaling of the modified Jiles–Atherton model," *Phys. B, Condens. Matter*, vol. 407, no. 13, pp. 2438–2441, Jul. 2012.
- [12] F. Henrotte and K. Hameyer, "A dynamical vector hysteresis model based on an energy approach," *IEEE Trans. Magn.*, vol. 42, no. 4, pp. 899–902, Apr. 2006.
- [13] K. Hergli, H. Marouani, M. Zidi, Y. Fouad, and M. Elshazly, "Identification of Preisach hysteresis model parameters using genetic algorithms," *J. King Saud Univ.-Sci.*, vol. 31, no. 4, pp. 746–752, 2017.

- [14] A. Iványi, Ed., *Preisach Memorial Book*, Budapest, Hungary: Akadémiai Kiadó, 2005.
- [15] Z. Wlodarski *et al.*, “Modeling DC-biased hysteresis curves in self-developed SMC cores,” *Int. J. Appl. Electromagn. Mech.*, vol. 61, no. S1, pp. S151–S157, 2019.
- [16] J. D. Jackson, *Classical Electrodynamics*, 3rd ed. New York, NY, USA: Wiley, 1999.
- [17] D. Jiles and D. Atherton, “Theory of ferromagnetic hysteresis,” *J. Magn. Magn. Mater.*, vol. 61, nos. 1–2, p. 48–60, 1986.
- [18] D. Jiles, J. Thoelke, and M. Devine, “Numerical determination of hysteresis parameters for the modeling of magnetic properties using the theory of ferromagnetic hysteresis,” *IEEE Trans. Magn.*, vol. 28, no. 1, pp. 27–35, Jan. 1992.
- [19] J. M. Jin, *The Finite Element Method in Electromagnetics*. New York, NY, USA: Wiley, 2002.
- [20] M. Kachniarz and R. Szewczyk, “Study on the Rayleigh hysteresis model and its applicability in modeling magnetic hysteresis phenomenon in ferromagnetic materials,” *Acta Phys. Polonica A*, vol. 131, no. 5, pp. 1244–1250, May 2017.
- [21] P. Kirkegaard and R. Brincker, “On the optimal location of sensors for parametric identification of linear structural systems,” *Mech. Syst. Signal Process.*, vol. 8, no. 6, pp. 639–647, Nov. 1994.
- [22] P. I. Koltermann *et al.*, “A modified Jiles method for hysteresis computation,” *Phys. B, Condens. Matter*, vol. 275, pp. 233–237, Jan. 2000.
- [23] M. Eusuff, K. Lansey, and F. Pasha, “Shuffled frog-leaping algorithm: A memetic meta-heuristic for discrete optimization,” *Eng. Optim.*, vol. 38, no. 2, pp. 129–154, Mar. 2006.
- [24] V. François-Lavet, F. Henrotte, L. Stainier, L. Noels, and C. Geuzaine, “An energy-based variational model of ferromagnetic hysteresis for finite element computations,” *J. Comput. Appl. Math.*, vol. 246, pp. 243–250, Jul. 2013.
- [25] J. Leite, N. Sadowski, P. Kuo-Peng, N. Batistela, and J. Bastos, “The inverse Jiles–Atherton model parameters identification,” *IEEE Trans. Magn.*, vol. 39, no. 3, pp. 1397–1400, May 2003.
- [26] J. Leite *et al.*, “Real coded genetic algorithm for Jiles–Atherton model parameters identification,” *IEEE Trans. Magn.*, vol. 40, no. 2, pp. 888–891, Mar. 2004.
- [27] J. V. Leite, A. Benabou, and N. Sadowski, “Accurate minor loops calculation with a modified Jiles–Atherton hysteresis model,” *Compel*, vol. 28, no. 3, pp. 741–749, 2009.
- [28] T. Matsuo, D. Shimode, Y. Terada, and M. Shimasaki, “Application of stop and play models to the representation of magnetic characteristics of silicon steel sheet,” *IEEE Trans. Magn.*, vol. 39, no. 3, pp. 1361–1364, May 2003.
- [29] T. Matsuo, Y. Terada, and M. Shimasaki, “Representation of minor hysteresis loops of a silicon steel sheet using stop and play models,” *Phys. B, Condens. Matter*, vol. 372, nos. 1–2, pp. 25–29, Feb. 2006.
- [30] L. Prigozhin, V. Sokolovsky, J. W. Barrett, and S. E. Zirka, “On the energy-based variational model for vector magnetic hysteresis,” *IEEE Trans. Magn.*, vol. 52, no. 12, pp. 1–11, Dec. 2016.
- [31] R. Naghizadeh, B. Vahidi, and S. H. Hosseini, “Parameter identification of Jiles–Atherton model using SFLA,” *Compel*, vol. 31, no. 4, pp. 1293–1309, Jul. 2012.
- [32] H. W. L. Naus, “Theoretical developments in magnetomechanics,” *IEEE Trans. Magn.*, vol. 47, no. 9, pp. 2155–2162, Sep. 2011.
- [33] N. Pop and O. Caltun, “Jiles–Atherton magnetic hysteresis parameters identification,” *Acta Phys. Pol. A*, vol. 120, no. 3, pp. 491–496, Sep. 2011.
- [34] C. Papadimitriou, J. L. Beck, and S.-K. Au, “Entropy-based optimal sensor location for structural model updating,” *J. Vib. Control*, vol. 6, no. 5, pp. 781–800, Jul. 2000.
- [35] J. Tellinen, “A simple scalar model for magnetic hysteresis,” *IEEE Trans. Magn.*, vol. 34, no. 4, pp. 2200–2206, Jul. 1998.
- [36] M. Toman, G. Stumberger, and D. Dolinar, “Parameter identification of the Jiles–Atherton hysteresis model using differential evolution,” *IEEE Trans. Magn.*, vol. 44, no. 6, pp. 1098–1101, Jun. 2008.
- [37] E. D. Torre, *Magnetic Hysteresis*. Hoboken, NJ, USA: Wiley, 1999.
- [38] F. E. Udawadia, “Methodology for optimum sensor locations for parameter identification in dynamic systems,” *J. Eng. Mech.*, vol. 120, no. 2, pp. 368–390, Feb. 1994.
- [39] G. Vertésy *et al.*, “Minor hysteresis loops measurements for characterization of cast iron,” *Phys. B, Condens. Matter*, vol. 372, nos. 1–2, pp. 156–159, 2006.
- [40] A. Vijn, E. Lepelaars, J. Dubbeldam, M. Van Gijzen, and A. Heemink, “Magnetic susceptibility estimation for magnetostatics,” *IEEE Trans. Magn.*, vol. 55, no. 3, pp. 1–9, Mar. 2019.
- [41] Y. Vuillemer *et al.*, “Scalar potential formulation and inverse problem applied to thin magnetic sheets,” *IEEE Trans. Magn.*, vol. 44, no. 6, pp. 1054–1057, Jun. 2008.
- [42] M. A. Zaman, P. C. Hansen, L. T. Neustock, P. Padhy, and L. Hesselink, “Adjoint method for estimating Jiles–Atherton hysteresis model parameters,” *J. Appl. Phys.*, vol. 120, no. 9, Sep. 2016, Art. no. 093903.
- [43] S. E. Zirka *et al.*, “On physical aspects of the Jiles–Atherton hysteresis models,” *J. Appl. Phys.*, vol. 112, no. 4, 2012, Art. no. 043916.
- [44] J. Ziske and T. Bödrich, “Magnetic hysteresis models for modelica,” in *Proc. 9th Int. Modelica Conf.*, 2012, pp. 151–158.